JOURNAL OF AIRCRAFT
Vol. 46, No. 1, January–February 2009

State-Space Modeling and Identification of Delta Wing Vortex-Coupled Roll Dynamics

Brandon W. Gordon*
Concordia University, Montréal, Québec H3G 1M8, Canada
Mehrdad Pakmehr†
Georgia Institute of Technology, Atlanta, Georgia 30332-0150
and
C. A. Rabbath‡
Defence Research and Development Canada,
Valcartier, Québec G3J 1X5, Canada

DOI: 10.2514/1.23596

This paper develops a new state-space model for vortex-coupled 65-degree delta wing aircraft systems based on a modified nonlinear indicial response method combined with an internal state-space representation. Relationships between vortex breakdown location, rolling moment coefficient, and roll angle dynamics are determined. The state-space equations derived are subject to state delays and are also nonlinear in the vortex-coupled rolling moment coefficient. Linear and nonlinear parameter identification methods are developed to empirically estimate the rolling moment coefficient as a function of the roll angle and primary vortex breakdown locations. A comparison between numerical simulations and experimental data indicates close agreement for a number of different initial conditions.

Nomenclature

A, B	=	circulation distribution parameters
$\mathbf{A}(t)$, $\mathbf{b}(t)$	=	equation terms in least-squares identification matrices
$\mathbf{A}_{\text{ls}}$, $\mathbf{x}_{\text{ls}}$, $\mathbf{b}_{\text{ls}}$	=	least-squares identification matrices
a	=	parameter for unsteady vortex effect
b_w	=	wing span
C_0	=	circulation distribution constant
C_l	=	rolling moment coefficient
c_w	=	wing chord
e_i	=	C_l correlation fitting parameters
f_c	=	friction coefficient
I_w	=	wing moment of inertia
k_q	=	parameter for quasi-steady vortex effect
N_p	=	number of points in a given experimental data set
Q, b, c	=	constants in the state-space model
q	=	dynamic air pressure
s_w	=	wing element area
T^*	=	release time
T	=	integration period for unsteady term in X_{vb}
t	=	time at observation
u_∞	=	freestream velocity
X_q	=	quasi-steady term in X_{vb}
X_s	=	static term in X_{vb}
X_u	=	indicial response function for the unsteady term in X_{vb}
X_{vb}	=	nondimensional vortex breakdown location
$\mathbf{x}$	=	state vector of system
α	=	angle of attack
β	=	sideslip angle
Γ	=	circulation or vortex strength
Γ_c	=	critical circulation
$\Delta\alpha$	=	bevel angle correction term
δ	=	bevel angle
Λ	=	effective sweep angle
Λ_0	=	leading-edge sweep angle
Λ_e	=	empirically obtained value of sweep back angle
λ_0	=	half-apex angle
ρ	=	air density
σ	=	effective roll-axis inclination
σ_0	=	roll-axis inclination
τ	=	time at step onset
ϕ	=	roll angle
ϕ_e	=	equilibrium roll angle
$\dot{\phi}$	=	roll rate

Subscripts

l	=	left vortex
q	=	quasi-steady term
r	=	right vortex
s	=	static term
u	=	unsteady term
vb	=	vortex breakdown
w	=	wing

I. Introduction

The high-angles-of-attack flight regime for delta wing aircraft systems often includes complex phenomena such as nonsteady flow, crossflow separation, and vortex breakdown. For situations when modern tactical fighters are forced into high-angles-of-attack flight regimes, it is potentially beneficial to take advantage of the nonlinear lift generated from vortices that form on their leeward sides. This may result in substantial improvement of aircraft maneuverability and performance. However, at sufficiently high angles of attack, vortex asymmetries can form and induce dynamic motions such as wing rock, sustained limit cycles, and yaw oscillation. Wing rock and other self-induced aircraft motions can be difficult to control and may result in departure from the desired flight envelope. Although many approaches have been proposed for wing rock, control of

Received 3 March 2006; revision received 31 January 2008; accepted for publication 5 February 2008.

*Associate Professor, Control and Information Systems Laboratory, Department of Mechanical and Industrial Engineering; bwgordon@encs.concordia.ca.

†Graduate Student, School of Aerospace Engineering. AIAA Student Member.

‡Defence Scientist.

vortex-coupled dynamic interactions has received considerably less attention by the aerospace research community. This is in part due to the current lack of low-order models suitable for control analysis and design. However, vortex coupling has great potential for improving the performance of delta wing aircraft, and there is significant need for state-space and control-oriented models in this area [1–3].

A number of methods can be found in the literature for simulation and modeling of vortex breakdown over delta wing aircraft, high-performance aircraft dynamics, and vortex flow regimes. These methods include computational, neural-network, and mathematical techniques. In [4], a parabolic distribution for the chordwise axial circulation distribution over a slender delta wing has been proposed. Leading-edge vortex breakdown locations have been predicted on the basis of a critical value for the circulation. A new method [5] has been proposed to predict the normal force coefficient acting on a delta wing under static and dynamic conditions. The three-dimensional Reynolds-averaged Navier–Stokes equations were used in [6] to numerically simulate the nonsteady vertical flow around a 65 deg sweep delta wing. In [7], the dynamic representation of an aerodynamic vortex lattice model has been investigated from a classical and system identification perspective. Furthermore, in [8], a conceptual model of vortex breakdown is proposed as a symmetry-breaking subcritical bifurcation from an axisymmetric unburst vortex to a helically symmetric translating spiral burst.

One of the main difficulties in determining the relationship between the instantaneous aerodynamic reactions on a maneuvering aircraft and the motion variables is the fact that the relationship is not solely determined by the instantaneous values of the motion variables. The instantaneous aerodynamic reactions generally depend on all of the prior state values up to the time instant in question [9]. To address this problem, the nonlinear indicial response (NIR) method was developed. This approach provides an extension to linear aerodynamic indicial functions and superposition concepts. The NIR method represents aerodynamic response variables, such as forces and moments, due to an arbitrary motion input as a summation of nonlinear responses to a series of step motions leading up to the step onset. Three important concepts are introduced in this approach: 1) a nonlinear indicial response functional, 2) a generalized superposition integral, and 3) under conditions where Frechet differentiability is lost (i.e., at a critical state), a split of the integral including a transient term [10–13].

In [14–21], the NIR method has been applied in numerous applications for modeling uncertain aerodynamics and nonlinear flight dynamics. Reisenthel [22] demonstrates the use of a time-domain Volterra kernel identification method which uses physically realizable inputs, and minimizes or eliminates the need for analytical assumptions. In [23], a study of aircraft aerodynamic equations with unsteady effects has been presented. The aerodynamic forces and moments have been expressed in terms of indicial functions or internal state variables. Other related works include [9,24–27]. A review of aerodynamic mathematical modeling for aircraft motions at high angles of attack is presented in [28]. The mathematical model defines a set of characteristic motions from which the aerodynamic response during a high-angle-of-attack flight maneuver can be predicted. In [29], a dynamic wind-tunnel test for a 65 deg swept delta wing has been reviewed and examined in light of the NIR theory. The existence of critical states with respect to roll angle has been reported. Further, [30] presents an investigation for the critical state transients of a 65 deg delta wing system. In [31], a state-space modeling approach based on NIR theory is developed, which is applicable to simulation and control system design. In this work, the vortex-coupled rolling moment coefficient is assumed to be a function of the roll angle.

Recently, a simulation model for vortex-coupled delta wing dynamics has been developed and verified experimentally [10,11,32]. It was found that, for delta wing systems, the leading-edge primary vortex has a dominant effect on resulting air loads. Consequently, the related air loads applied to the surface of the delta wing can be calculated in terms of the primary vortex breakdown locations. To model the vortex dynamics, a nonlinear indicial response and internal state-space (NIRISS) approach was employed. However, the representation developed requires an iterative solution to determine the rolling moment coefficient. It also contains unsteady integral terms that are a function of delayed roll velocities. As a result, the method is not in an explicit state variable form required by most control design methods.

In this paper, a new explicit state-space model for vortex-coupled delta wing aircraft systems is developed. The dynamic representation includes state delays and uncertainty in the vortex-coupled rolling moment coefficient. This result is achieved using a new state variable formulation that allows the distributed delay terms in the NIRISS representation to be expressed using discrete time-delay differential equations. This method provides a model that is applicable to a wide variety of control analysis and design methods for state-space systems with time delays [33]. The distributed delay terms in previous NIRISS applications limited the applicability of this approach to a much smaller class of control methods [33]. Furthermore, this paper represents the first state-space modeling approach to represent the rolling moment coefficient as an explicit function of the left and right vortex breakdown locations. In most of the previous research related to delta wing roll dynamics, the rolling moment coefficient is assumed to be a function of the roll angle [29–31,34–36] or it was obtained through iterative calculations of the flowfield pressure distribution [10,11,32]. In the work of [5,37–39], the concept of rolling moment dependency on vortex breakdown location is proposed, but no state-space mathematical model is developed.

To obtain a more accurate dynamic model, in this paper, it is assumed that the rolling moment coefficient is a function of the left and right vortex breakdown locations. It is shown that this new approach provides substantially better agreement with experimental data. Linear, nonlinear, and static parameter identification methods are developed to empirically estimate the rolling moment coefficient and its uncertainty bound from experimental data. A comparison between numerical simulations and experimental data indicates close agreement for a number of different initial conditions. This experimentally validated state-space model represents a significant step toward a control-oriented model for vortex-coupled delta wing systems. The experimental data currently available provided validation of the proposed model for open-loop initial condition response tests. In future work, the proposed model will be experimentally validated for conditions with control inputs applied to the system.

II. Description of Delta Wing Vortex-Coupled System

A comprehensive experimental study has been previously conducted to determine the flow physics of vortex-coupled delta wing systems in the roll direction. The results of this investigation performed at the National Research Council Canada, Institute for Aerospace Research are presented in [10,11,32]. Experimental data from this investigation were used for identification and verification of the model developed in this paper. The experiments were conducted using 2×3 m and 7×10 ft wind tunnels. Figure 1 shows the 65 deg delta wing model. The experimental setup is illustrated in Fig. 2. The delta wing is constrained to the roll direction by a set of bearings. An input torque can be applied using a servomotor, and the position can be measured using an encoder. For certain flow conditions, vortices will form on the two sides of the delta wing.

Experiments carried out for flows at high incidence [10,11] indicate that there may exist primary, secondary, and tertiary vortices over the delta wing. The presence of leading-edge vortices and, particularly, their primary breakdown location along the wing is the main cause of air load nonlinearities and time dependence. It was determined that the effect of secondary and tertiary vortices on air loads is second order compared with the primary vortices. Therefore, the effect of secondary and tertiary vortices are ignored in this investigation. It should also be noted that the delta wing model used in the experimental investigation is a 65 deg delta wing, not a slender delta wing. Therefore, dynamic wing rock phenomena is not as important for this problem compared with slender delta wing systems.

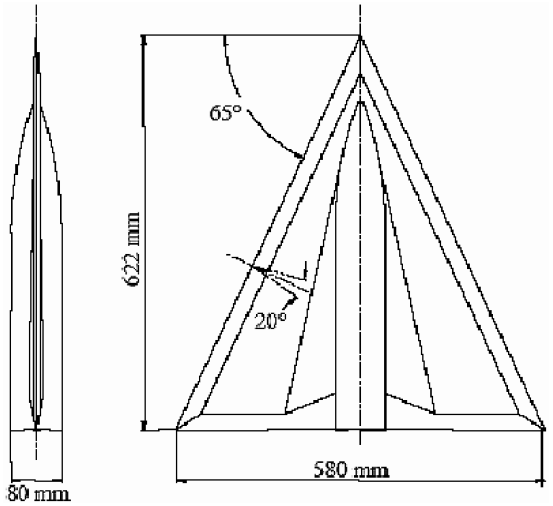

Fig. 1 Delta wing model (65 deg) [11].

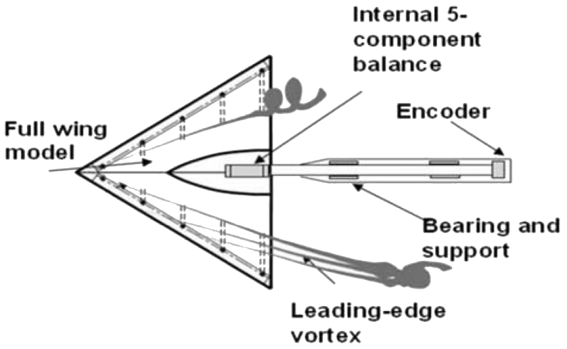

Fig. 2 Delta wing experimental setup [49].

For the experiments performed, the delta wing was allowed to move freely about the roll axis. The initial condition response was found by releasing the delta wing from an initial roll angle with zero initial angular velocity. It was found that, for a nominal freestream velocity of $u_\infty = 91$ m/s, the delta wing apparatus has multiple stable equilibrium points depending on the roll-axis inclination σ_0 [10,11]. The experimental data available from [10,11] can be categorized into four different types. The categories associated with the initial roll angle and equilibrium points are indicated in Table 1.

The objective of the proposed modeling work is to capture the dynamic behavior observed for these cases. This includes prediction of the roll angle response and the rolling moment coefficient, including the dependency on the roll angle and vortex breakdown locations. The modeling approach developed in the following sections will address this problem.

III. State-Space Formulation of the System

An explicit state-space model is developed in this section based on the NIRISS representation of vortex-coupled delta wing dynamics proposed in [10,11,32].

Table 1 Different categories of experimental data

Category no.	Initial roll angle	Equilibrium point
1	Positive	Positive
2	Positive	Close to zero
3	Negative	Close to zero
4	Negative	Negative

A. Derivation of State-Space Formulation

According to the NIRISS method [10,11], the dimensionless vortex breakdown location over a delta wing is given by

$$X_{\text{vb}} = X_s[\phi(t)] + X_q[\dot{\phi}(t)]X_s[\phi(t)] + \int_{t-T}^{t} X_u(t-\tau)\dot{\phi}(\tau)\,\mathrm{d}\tau \quad (1)$$

where the first term represents the static value at time t. The second and third terms reflect the quasi-steady and unsteady effects, respectively. It should be noted that, for the NIRISS method, the convolution integral is limited to the domain $[t-T, t]$. This assumption implies that only the last T s of the motion time history has any direct effect on the vortex breakdown locations. A discussion of this important assumption is provided later in this section after the form of $X_u(t-\tau)$ is proposed in Eq. (20).

The locations of the right and left vortices over the delta wing are calculated from

$$X_{\text{vbr}} = X_{\text{sr}}[\phi(t)] + X_q[\dot{\phi}(t)]X_{\text{sr}}[\phi(t)] + \int_{t-T}^{t} X_u(t-\tau)\dot{\phi}(\tau)\,\mathrm{d}\tau \quad (2)$$

$$X_{\text{vbl}} = X_{\text{sl}}[\phi(t)] - X_q[\dot{\phi}(t)]X_{\text{sl}}[\phi(t)] - \int_{t-T}^{t} X_u(t-\tau)\dot{\phi}(\tau)\,\mathrm{d}\tau \quad (3)$$

The difference between X_{vbr} and X_{vbl} are the static terms X_{sr} and X_{sl}. The unsteady integral terms have the same formulation, but are of opposite signs [10,11]. The quasi-steady related terms also have opposite signs. The signs of the individual terms in Eqs. (2) and (3) were checked by comparing their output with data from existing work [10,11,40,41]. It should also be noted that, due to symmetry in the problem, the following relationship between the left and right vortex locations will be satisfied:

$$X_{\text{vbl}}(\phi(t), \dot{\phi}(t)) = X_{\text{vbr}}(-\phi(t), -\dot{\phi}(t)) \quad (4)$$

The magnitude and sign of the individual terms in Eqs. (2) and (3) were found to be consistent with this relationship.

Figure 3 shows a schematic representation of vortex breakdown locations on the delta wing and its effect on the rolling moment. The left and right vortex breakdown locations are dimensionless parameters that vary from 0 (leading edge) to 1 (trailing edge) when the breakdown location occurs on the wing. In this paper, it is assumed that the two vortex breakdown location motions are independent of each other. Some investigations have found that coupling between the left and right vortex breakdown locations can occur in various situations. In [42], it was found that a streamwise instability mechanism can result in low-amplitude and low-frequency coupled oscillations between the left and right vortex locations. This type of phenomena was not observed for the experimental conditions modeled in this paper. The high-amplitude and high-frequency oscillations associated with the independent vortex breakdown terms appeared to be the most significant mechanisms involved with the system dynamics. Comparison of the model response to the experimental data confirmed this notion. However, in some cases, the coupling effects might be considered significant. This could be an interesting direction for future research if suitable experimental conditions are available to produce significant coupling interactions.

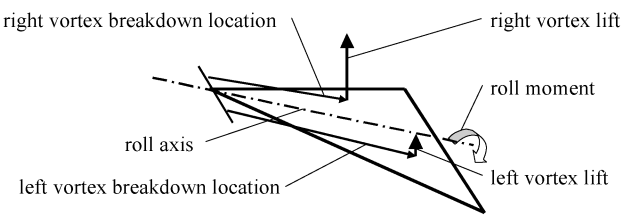

Fig. 3 Illustration of vortex breakdown on delta wing surface.

The quasi-steady related term X_q is given by

$$X_q = k_q(t)\dot{\phi}(t) \tag{5}$$

where k_q is an empirically obtained correlation [10,11]

$$k_q(t) = 0.91/\tan[\alpha(t)] \tag{6}$$

where the angle of attack is given by

$$\alpha(t) = \text{a}\tan\{\cos[\phi(t)]\tan(\sigma)\} \tag{7}$$

The static term X_s is approximated using the parabolic form

$$\Gamma_c = C_0 + BX_s - AX_s^2 \tag{8}$$

where A, B, C_0, and Γ_c are parameters that can be obtained from the following empirically derived expressions [10,11,32]. The expressions for the left and right static terms X_s are the same, except for the effective sweep back angle Λ indicated as follows:

$$\Lambda_l = \lambda_0 - \text{a}\tan\{\tan(\sigma)\sin[\phi(t)]\} \tag{9}$$

$$\Lambda_r = \lambda_0 + \text{a}\tan\{\tan(\sigma)\sin[\phi(t)]\} \tag{10}$$

where λ_0 is the half-apex angle. The parameter σ is the effective roll-axis inclination given by

$$\sigma = \sigma_0 - \Delta\alpha \tag{11}$$

where σ_0 is the roll-axis inclination and $\Delta\alpha$ is a bevel angle correction term. This correction term is analogous to the angle-of-attack correction described in [43]. For the model in this paper, $\Delta\alpha$ is assumed to be a constant that can be determined experimentally for a given nominal sweep angle, bevel angle, and roll-axis inclination. This allows a more accurate determination of $\Delta\alpha$ than using a published correlation.

The values of A and B are obtained using

$$A = 1.1\sin[\alpha(t)]\sin[\Lambda(t)] \qquad B = 4A \tag{12}$$

The critical circulation values are expressed as

$$\Gamma_c = 0.8\cos\{4[\Lambda(t) - \Lambda_e]\} \tag{13}$$

where Λ_e was determined experimentally to be

$$\Lambda_e = 20/57.3 \text{ rad} \tag{14}$$

The nondimensional circulation at the trailing edge is used to determine the distributions of circulation in the chordwise direction using a parabolic form [10,11]. This provides

$$C_0 = \Gamma - B + A \tag{15}$$

where

$$\Gamma = 5.11[\Lambda(t) + 2.65/57.3][\alpha(t) - 3.5/57.3] \tag{16}$$

The solution of the static term X_s can now be determined from Eq. (8) as follows:

$$X_s(t) = \frac{B - \sqrt{|B^2 + 4A(C_0 - \Gamma_c)|}}{2A}, \qquad B^2 + 4A(C_0 - \Gamma_c) \geq 0 \tag{17}$$

otherwise,

$$X_s(t) = \frac{B + \sqrt{|B^2 + 4A(C_0 - \Gamma_c)|}}{2A}, \qquad B^2 + 4A(C_0 - \Gamma_c) < 0 \tag{18}$$

To develop explicit state variable equations, the unsteady integral term in Eq. (1) needs to be expressed in differential form. This distributed delay expression can be transformed to differential equation form using the state variable formulation described next. Consider the unsteady integral term of Eq. (1) defined by

$$J_u = \int_{t-T}^{t} X_u(t-\tau)\dot{\phi}(\tau)\,\mathrm{d}\tau \tag{19}$$

The indicial response function $X_u(t-\tau)$ can be obtained from [10,11]

$$X_u(t-\tau) = \frac{1.65}{\tan\alpha(t)}\sin\left(\frac{\pi(t-\tau)}{T^*}\right), \qquad t - T^* \leq \tau \leq t$$
$$X_u(t-\tau) = 0, \qquad \tau < t - T^* \tag{20}$$

where T^* is the release time. The release time is the width of the indicial response function $X_u(t-\tau)$. Outside of the domain $[t - T^*, t]$ the indicial response function is assumed to be zero. In general, the release time could vary with time for a given problem. To facilitate the model derivation and identification, a simplifying assumption was made that the release time is constant. This could be interpreted as an average release time for the system. For this case, the integral domain parameter can be equated to the release time

$$T = T^* \tag{21}$$

since $X_u(t-\tau) = 0$ before a time of $t - T^*$ in the integral expression (19). In mathematical terms, the release time represents the period of decay of the indicial response function. Thus, the assumption can be interpreted as the indicial response function converging closely to zero after a release time T^*. Justification for this assumption comes from the fact that an indicial response for a stable system will converge to a steady-state value after a given time [44,45]. For the NIRISS approach, the static vortex term accounts for the steady-state value, and so the corresponding indicial response component will converge to zero at steady state. This also implies that the convolution integral (19) only needs to be made over the last T s. In other words, for this assumption, only the last T s of the motion time history has any direct effect on the vortex breakdown locations. This idea of limited system memory is also often employed by other references that use the nonlinear indicial response method [12,13], where it is used to reduce the indicial response functional that depends on the entire time history to a parameter dependent function.

The motivation for the release-time assumption is because it reduces the required domain of the convolution integral. This results in less computational requirements and a more mathematically tractable expression for modeling and system identification purposes. The half-sine indicial response function shape was chosen because it is a mathematically simple expression that converges to zero after the release time, and also because the response of the NIRISS model with this shape provided good agreement to experimental data for the roll angle response and the rolling moment coefficient [10,11]. Furthermore, because it is zero at the end points of the integral domain, it promotes a higher degree of numerical continuity in the NIRISS response because there is no truncation of the indicial response function by the integral bounds. It should be noted that using the half-sine indicial response function (20) and integrating it over the last T s in Eq. (19) are key assumptions that facilitate the derivation of the proposed state-space model in this paper. This results in a relatively simple unsteady vortex term, which only depends on the last T s of motion history. In Sec. V.C, it is shown that the resulting expressions for the vortex terms in Eqs. (2) and (3) allow significantly better agreement with experimental data compared with only using static functions of ϕ for the rolling moment coefficient.

Equation (20) can now be represented as follows:

$$X_u(t-\tau) = a(t)\sin[c(t-\tau)] \tag{22}$$

where

$$a(t) = 1.65/\tan[\alpha(t)] \tag{23}$$

$$c = \pi/T^* = \pi/T \tag{24}$$

Expanding Eq. (22) yields

$$X_u(t-\tau) = a(t)\sin(ct)\cos(c\tau) - a(t)\cos(ct)\sin(c\tau) \tag{25}$$

By substituting $X_u(t-\tau)$ from Eq. (25) into Eq. (19), the integral term can be represented as

$$J_u = a(t)\sin(ct)z_1(t) - a(t)\cos(ct)z_2(t) \tag{26}$$

where

$$z_1(t) = \int_{t-T}^{t} \cos(c\tau)\dot{\phi}(\tau)\,\mathrm{d}\tau, \qquad z_2(t) = \int_{t-T}^{t} \sin(c\tau)\dot{\phi}(\tau)\,\mathrm{d}\tau \tag{27}$$

In other words,

$$J_u = a(t)x_1(t) \tag{28}$$

where

$$x_1(t) = \sin(ct)z_1(t) - \cos(ct)z_2(t) \tag{29}$$

Differentiating $x_1(t)$ with respect to time gives

$$\dot{x}_1(t) = \sin(ct)\dot{z}_1(t) - \cos(ct)\dot{z}_2(t) + cx_2(t) \tag{30}$$

where

$$x_2(t) = \cos(ct)z_1(t) + \sin(ct)z_2(t) \tag{31}$$

Combining Eqs. (29) and (31) gives

$$\begin{bmatrix} x_1(t) \\ x_2(t) \end{bmatrix} = \begin{bmatrix} \sin(ct) & -\cos(ct) \\ \cos(ct) & \sin(ct) \end{bmatrix} \begin{bmatrix} z_1(t) \\ z_2(t) \end{bmatrix} \tag{32}$$

Inverting this nonsingular relationship yields

$$\begin{bmatrix} z_1(t) \\ z_2(t) \end{bmatrix} = \begin{bmatrix} \sin(ct) & \cos(ct) \\ -\cos(ct) & \sin(ct) \end{bmatrix} = \begin{bmatrix} x_1(t) \\ x_2(t) \end{bmatrix} \tag{33}$$

The derivatives of $z_1(t)$ and $z_2(t)$ in Eq. (27) can be expressed as

$$\begin{aligned} \dot{z}_1(t) &= \cos(ct)\dot{\phi}(t) - \cos[c(t-T)]\dot{\phi}(t-T) \\ \dot{z}_2(t) &= \sin(ct)\dot{\phi}(t) - \sin[c(t-T)]\dot{\phi}(t-T) \end{aligned} \tag{34}$$

The following roll angle motion states are now defined as

$$x_3(t) = \phi(t) \tag{35}$$

$$x_4(t) = \dot{\phi}(t) \tag{36}$$

Equation (34), expressed in matrix form, gives

$$\begin{bmatrix} \dot{z}_1(t) \\ \dot{z}_2(t) \end{bmatrix} = \begin{bmatrix} \cos(ct) & -\cos(ct) \\ \sin(ct) & -\sin(ct) \end{bmatrix} \begin{bmatrix} x_4(t) \\ x_4(t-T) \end{bmatrix} \tag{37}$$

Differentiating $x_1(t)$ and $x_2(t)$ in Eq. (32), with respect to time, yields

$$\begin{bmatrix} \dot{x}_1(t) \\ \dot{x}_2(t) \end{bmatrix} = \begin{bmatrix} c\cos(ct) & c\sin(ct) \\ -c\sin(ct) & c\cos(ct) \end{bmatrix} \begin{bmatrix} z_1(t) \\ z_2(t) \end{bmatrix} + \begin{bmatrix} \sin(ct) & -\cos(ct) \\ \cos(ct) & \sin(ct) \end{bmatrix} \begin{bmatrix} \dot{z}_1(t) \\ \dot{z}_2(t) \end{bmatrix} \tag{38}$$

Finally, combining Eqs. (33), (37), and (38), after simplification, gives

$$\dot{x}_1(t) = cx_2(t) \qquad \dot{x}_2(t) = -cx_1(t) + x_4(t) + x_4(t-T) \tag{39}$$

The equation of motion in the roll direction is given by

$$I_w\ddot{\phi}(t) = C_l(t)qs_wb_w - f_c\dot{\phi}(t) + u(t) \tag{40}$$

where $u(t)$ is an external input torque applied to the delta wing in the roll direction. The coefficient f_c represents the viscous friction due primarily to the bearings in the apparatus. Equations (39) and (40) represent a set of differential equations that describe the vortex-coupled delta wing system. The rolling moment coefficient $C_l(t)$ will vary with the vortex breakdown locations, which, in turn, will depend on the states of the system. The elimination of the distributed delayed integral expression from the NIRISS formulation, using Eq. (39), provides an explicit state variable model that is much better suited for control analysis and design [33] than previous NIRISS formulations.

B. Summary of the State-Space Formulation

1. *Definition of State Variables*

The integral term of X_{vb} in Eq. (1) is represented by $a(t)x_1(t)$. The term $\dot{x}_1(t)$ from Eq. (30) is represented by $x_2(t)$. The roll angle $\phi(t)$ and velocity $\dot{\phi}(t)$ are expressed as $x_3(t)$ and $x_4(t)$, respectively.

2. *Vortex Breakdown Locations in State Variable Form*

The vortex breakdown locations in state variable form are given by

$$X_{\mathrm{vbr}}(t) = X_{\mathrm{sr}}[x_3(t)] + X_{\mathrm{sr}}[x_3(t)]k_q[x_3(t)]x_4(t) + a[x_3(t)]x_1(t) \tag{41}$$

$$X_{\mathrm{vbl}}(t) = X_{\mathrm{sl}}[x_3(t)] - X_{\mathrm{sl}}[x_3(t)]k_q[x_3(t)]x_4(t) - a[x_3(t)]x_1(t) \tag{42}$$

3. *State Variable Equations*

The equations previously developed can be expressed in a concise state variable form as follows:

$$\begin{aligned} \dot{x}_1(t) &= cx_2(t) & \dot{x}_2(t) &= -cx_1(t) + x_4(t) + x_4(t-T) \\ \dot{x}_3(t) &= x_4(t) & \dot{x}_4(t) &= QC_l(x) - bx_4(t) + u(t)/I_w \end{aligned} \tag{43}$$

where $Q = qs_wb_w/I_w$, $b = f_c/I_w$, and $u(t)$ is the external input torque.

IV. Parameters and Calculations

The aircraft characteristics and parameters in Table 2 have been obtained and calculated from the data reported in [10,11].

V. Parameter Identification

The majority of parameters in the proposed model, Eqs. (41–43), can be calculated based on geometry and other system properties. However, the rolling moment coefficient C_l is difficult to accurately calculate in this manner. The C_l parameter is a function of other state variables and it is also highly uncertain. Therefore, it is better to obtain this parameter through a system identification procedure [46].

Table 2 Aircraft characteristics and parameters

Half-apex angle	$\lambda_0 = 0.436$ rad
Leading-edge sweep angle	$\Lambda_0 = 1.134$ rad
Roll-axis inclination	$\sigma_0 = 0.523$ rad
Bevel angle	$\delta = 0.349$ rad
Bevel angle correction term	$\Delta\alpha = 0.090$ rad
Normalized chord	$c_w = 1$
Wing span	$b_w = 2\tan(\lambda_0)c_w = 0.933$
Wing area	$s_w = 0.18$ m^2
Freestream velocity	$u_\infty = 91$ m/s
Air density	$\rho = 1.2$ kg/m^3
Dynamic air pressure	$q = 0.5\rho u_\infty^2$
Moment of inertia	$I_w = 0.0305$ kg $\cdot$ m^2
Friction coefficient	$f_c = 0.124$ kg $\cdot$ m^2/s

In this paper, C_l is estimated using the following model structures: 1) linear least-squares approximation, 2) Nth-order polynomial approximation, and 3) static approximation. A radial basis function neural-network [47,48] structure with left and right vortex inputs was also attempted, but there was insufficient training data to satisfactorily identify the large number of network parameters. This resulted in good agreement with experimental C_l training values but poor agreement when the model was simulated, due to the inability of the network to predict C_l for significant perturbations from the training data trajectories.

The aforementioned model structures were identified using two data sets that consist of initial condition (IC) responses with no input applied. The first data set (IC 1) had initial conditions of $\phi(t) = -1.12$ rad for all $t \leq 0$ with an equilibrium point of $\phi_e = -0.02$ rad. This data set was used to estimate the parameters for the $\phi_e = -0.02$ rad equilibrium point. The second data set (IC 2) had initial conditions of $\phi(t) = -0.89$ rad for all $t \leq 0$ with an equilibrium point of $\phi_e = -0.36$ rad. This data set was used to estimate the parameters for the $\phi_e = -0.36$ rad equilibrium point. For the model structures investigated in this paper, it was found that each equilibrium point requires a different set of parameters which can be identified with an appropriate data set. Therefore, the proposed model is not capable of modeling multiple equilibrium behavior with one set of parameters. The coefficients of the model structures for each data set (IC 1 and IC 2) were identified, including estimates on the error bounds for those parameters. Furthermore, the model was validated by comparing the output of the identified model to two different data sets (IC 3 and IC 4) that were not used in the identification process. The details and results of the identification procedure are presented in this section. The validation process is presented in Sec. VI.

In most of the previous research related to delta wing roll dynamics, the rolling moment coefficient is assumed to be primarily a function of the roll angle [29–31,34–36]. In this paper, to obtain a more accurate dynamic model, it is assumed that C_l is also a function of the left and right vortex breakdown locations. The motivation for this formulation is based on the knowledge that the vortex breakdown locations lead to a difference in local pressure distributions on each side of the delta wing and, consequently, result in an overall moment represented by C_l. During dynamic interactions, the left and right vortex breakdown locations may not necessarily be functions of the roll angle. Therefore, the more general approach used in this paper will lead to a more accurate approximation of C_l for dynamic interactions. This fact will be demonstrated by a comparison of $C_l(\phi, X_{\text{vbr}}, X_{\text{vbl}})$ and $C_l(\phi)$ approximations in Sec. V.C.

A. Linear Least-Squares Approximation

For this case, C_l is approximated by the following linear correlation:

$$C_l(\phi, X_{\text{vbr}}, X_{\text{vbl}}) = e_0 + e_1\phi + e_2(X_{\text{vbl}} - X_{\text{vbr}}) \tag{44}$$

where e_i are fitting parameters. These parameters were identified by performing a least-squares curve fit to experimental data. Equation (44) can be expressed as

$$\begin{aligned} &\mathbf{A}(t)\mathbf{x}_{ls} = \mathbf{b}(t) \qquad \mathbf{x}_{\text{ls}} = \begin{bmatrix} e_0 & e_1 & e_2 \end{bmatrix}^T \\ &\mathbf{A}(t) = \begin{bmatrix} 1 & \phi & (X_{\text{vbl}} - X_{\text{vbr}}) \end{bmatrix}, \qquad \mathbf{b}(t) = [C_l] \end{aligned} \tag{45}$$

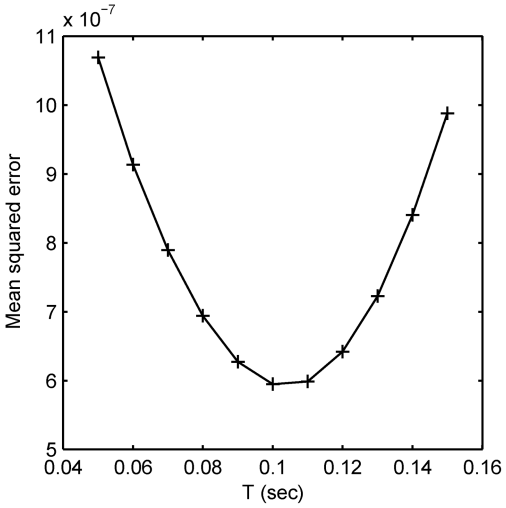

Fig. 4 Estimation mean squared error vs T (linear, IC 1).

The least-squares identification problem can then be formulated as an overdetermined linear system:

$$\mathbf{A}_{\text{ls}}\mathbf{x}_{ls} = \mathbf{b}_{\text{ls}} \qquad \mathbf{A}_{\text{ls}} = \begin{bmatrix} \mathbf{A}(t_1) \\ \mathbf{A}(t_2) \\ \vdots \\ \mathbf{A}(t_{N_p}) \end{bmatrix}, \qquad \mathbf{b}_{\text{ls}} = \begin{bmatrix} \mathbf{b}(t_1) \\ \mathbf{b}(t_2) \\ \vdots \\ \mathbf{b}(t_{N_p}) \end{bmatrix} \tag{46}$$

where N_p is the number of points in a given experimental data set. Note that X_{vbr}, X_{vbl}, and C_l in Eq. (45) are determined from experimental encoder-based measurements of $\phi(t)$ using Eqs. (2), (3), and (40), respectively. The velocity and acceleration terms in these expressions were estimated using center finite difference approximations. The unsteady integral term was estimated using trapezoidal numerical integration.

The overdetermined linear system (46) was solved using a pseudoinverse solution for each of the two data sets (IC 1 and IC 2). The result is a set of parameters e_i that minimizes the mean squared error between the C_l correlation (44) and the experimental data sets. To estimate T, plots of the mean squared identification error versus T were made for each data set. The result for IC 1 is illustrated in Fig. 4. It is evident that the estimation error for this case is minimized for $T = 0.10$ s. A similar procedure was performed to identify the optimal value of T for the other cases presented in this section. The results of the identification process for the linear structure are provided in Table 3.

The estimated error bounds for the parameters were determined by performing the identification process for other data sets and calculating the maximum deviation in the estimated parameters. Figure 5 shows the experimental C_l time history and its linear approximation for IC 1. It can be seen that the linear approximation has some significant deviations from the experimental data, especially during the initial phase of the response and also in the peak values. Figure 6 shows the corresponding roll angle time history and the simulation response for the linear approximation. It is evident that the errors in C_l result in a roll angle response with a slow rise time and low peak values. The initial phase of the response shows a significant deviation from the experimental data. The period of oscillation is also smaller than the experimental data. The equilibrium value was

Table 3 Estimated model parameters for linear C_l approximation

Parameter	IC 1, $\phi_e = -0.02$ rad	Error bounds	IC 2, $\phi_e = -0.36$ rad	Error bounds
T, s	0.10	±0.01	0.10	±0.01
e_0	−0.0011	±10.4205	−125.1045	±11.9671
e_1, rad^{-1}	−874.6448	±20.7912	−553.5100	±78.5028
e_2	−94.7339	±18.6101	−33.8574	±19.0496

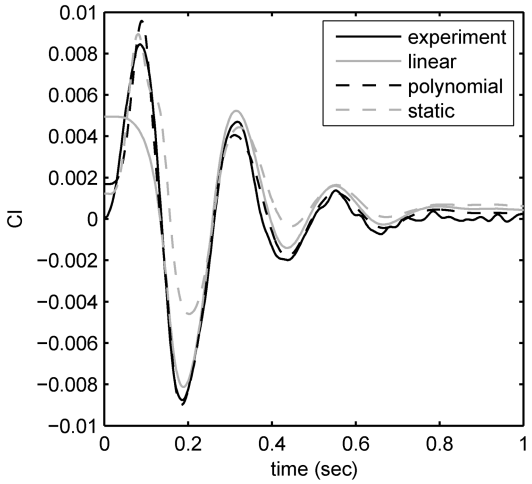

Fig. 5 Linear, polynomial, and static approximation of C_l (IC 1).

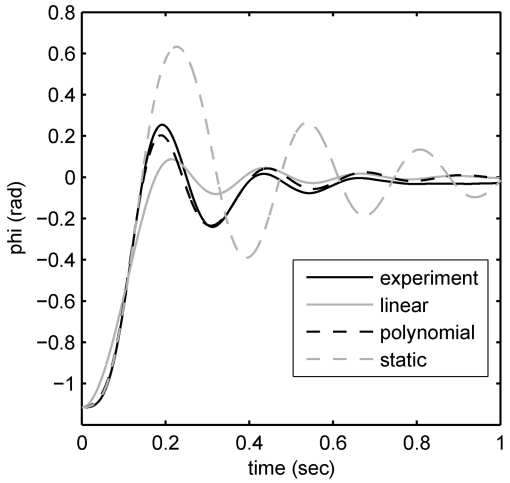

Fig. 6 Roll angle response using linear, polynomial, and static approximation (IC 1).

accurate. The results for IC 2 are shown in Figs. 7 and 8. It can be seen that, for this case, there are also significant errors in the C_l approximation during the initial phase of the response. The roll angle response shows a low initial peak value. However, the subsequent peak values are too large due to insufficient damping in the later part of the response. The period of oscillation is accurate in the initial

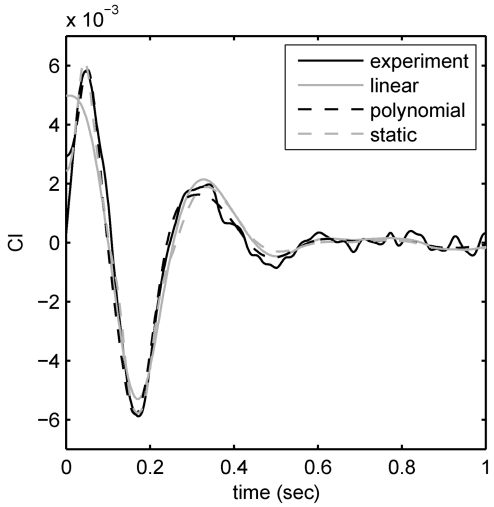

Fig. 7 Linear, polynomial, and static approximation of C_l (IC 2).

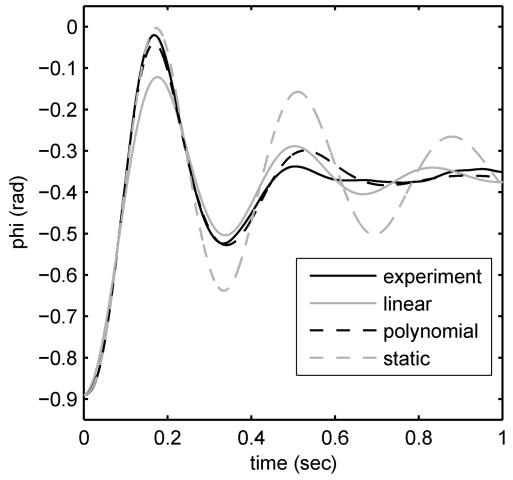

Fig. 8 Roll angle response using linear, polynomial, and static approximation (IC 2).

phase of the response and the equilibrium point is also close. It is apparent from the results for both data sets that there are significant errors in the linear approximation approach. This motivates the use of the *N*th-order polynomial approach presented in the following section.

B. *N*th-Order Polynomial Approximation

To obtain a better approximation for the nonlinearity in the C_l correlation, the following *N*th-order polynomial was employed:

$$C_l(\phi, X_{\text{vbr}}, X_{\text{vbl}}) = e_0 + e_1\phi + \sum_{i=1}^{N} e_{i+1}\left(X_{\text{vbl}}^i - X_{\text{vbr}}^i\right) \tag{47}$$

where e_i are the fitting parameters. Equation (47) can be expressed as

$$\begin{aligned} \mathbf{A}(t)\mathbf{x}_{\text{ls}} &= \mathbf{b}(t) \qquad \mathbf{x}_{\text{ls}} = \begin{bmatrix} e_0 & e_1 & e_2 & \cdots & e_{N+1} \end{bmatrix}^T \\ \mathbf{A}(t) &= \begin{bmatrix} 1 & \phi & (X_{\text{vbl}} - X_{\text{vbr}}) & \cdots & \left(X_{\text{vbl}}^N - X_{\text{vbr}}^N\right) \end{bmatrix} \\ \mathbf{b}(t) &= [C_l] \end{aligned} \tag{48}$$

The least-squares identification problem was formulated as an overdetermined system (46) and solved using a pseudoinverse approach in the same manner as the previous section. A fifth-order polynomial was found to provide good agreement with experimental data. The results of the parameter estimation process are presented in Table 4.

Figure 5 shows the C_l time history for the fifth-order approximation for IC 1. Figure 6 shows the corresponding roll angle time history. It can be seen that the polynomial approximation of C_l is significantly closer to the experimental data than the linear approximation, especially during the initial phase of the response. The peak values are also more accurate. As a result, the roll angle response is also more accurate during the initial part of the response. It is further evident that the oscillation period is close to the experimental data. The final part of the response, including the equilibrium point, is also accurate, although the damping is too small at the end of the response. The results for IC 2 are shown in Figs. 7 and 8. It is apparent that the polynomial approximation of C_l is a significant improvement over the linear approximation, especially during the initial phase of the response. The roll angle response is significantly more accurate both in the initial and final parts of the response. The damping is also more accurate in the final part of the response. The period of oscillation is slightly larger than the experimental data though, and there is also a small deviation at 0.5 s. However, the overall agreement to the experimental data is good and the accuracy is significantly better than the linear approximation. It is apparent from the results for both data sets that the polynomial approach provides significantly better agreement than the linear

Table 4 Estimated model parameters for polynomial C_l approximation

Parameter	IC 1, $\phi_e = -0.02$ rad	Error bounds	IC 2, $\phi_e = -0.36$ rad	Error bounds
T, s	0.11	±0.005	0.12	±0.01
e_0	0.0013	±1.2214	−67.1664	±40.3003
e_1, rad^{-1}	−832.4707	±26.4025	−823.8778	±180.9222
e_2	44.9291	±29.5905	9.5932	±5.0335
e_3	−176.9133	±86.0401	−113.1062	±26.2987
e_4	53.6139	±27.1442	28.7747	±26.5864
e_5	−6.8358	±3.9980	−1.2848	±1.6531
e_6	0.2501	±0.1823	−0.2416	±0.5181

approximation method. Therefore, the fifth-order polynomial approximation for C_l is the recommended model structure for the investigation in this paper.

An estimate of the model uncertainty bound for the fifth-order C_l approximation was determined from the error between the correlation and the experimental data for Figs. 5 and 7. From this information, it was determined that the uncertainty in C_l could be bounded by the following equation:

$$|C_l - \hat{C}_l| \leq \Delta, \qquad \Delta = 0.001645 \tag{49}$$

where C_l and $\hat{C}_l$ represent the experimental value and fifth-order polynomial estimate, respectively. Therefore, there is significant uncertainty in the system that would motivate the need for robust control development for vortex-coupled delta wing systems in future work.

C. Static Approximation

To determine the importance of using the vortex breakdown locations in the model structure an Nth-order polynomial in the roll angle was also identified and tested:

$$C_l(\phi) = e_0 + \sum_{i=1}^{N} e_i \phi^i \tag{50}$$

A comparison of this static modeling approach ($N = 7$) to the other approaches for IC 1 is shown in Figs. 5 and 6. It can be seen that the agreement for C_l is good for the initial part of the response, but, after the first peak, the accuracy reduces considerably, especially at the peak values. The roll angle response is only accurate during the very initial part of the response before the first peak. After that, the deviation is quite large with peaks that are too large and damping that is too small. The period of oscillation is also too large. The results for IC 2 are shown in Figs. 7 and 8. The agreement for C_l is relatively good compared with the linear and polynomial approaches. However, that does not translate into an accurate roll response. It can be seen that the peaks are too large and the damping is too small, although the period of oscillation is fairly accurate. This is a good example of how an accurate C_l approximation does not necessarily lead to a good agreement in roll angle response if the physics are not accurately accounted for in the correlation terms. From this section, it is evident that using vortex breakdown locations in the C_l correlation provides a significant improvement compared to using a static C_l function that depends solely on the roll angle.

VI. Comparison to Experimental Results

The proposed model, with the fifth-order C_l approximation from Sec. V.B, was validated in this section by comparing the simulation output of the identified model to two different data sets (IC 3 and IC 4) that were not used in the identification process of Sec. V.B. Both data sets represent initial condition responses with zero input applied. The numerical simulations were performed in a MATLAB M-file computational environment using Euler's method with a step size of 0.2 ms. The computational work space recorded the time history of every state, so that the time delayed states could be obtained by accessing previous states in the memory buffer. It was found that this approach was straightforward to implement with good accuracy and numerical stability properties.

The data set for IC 3 had initial conditions of $\phi(t) = 1.02$ rad for all $t \leq 0$ with an equilibrium point of $\phi_e = -0.02$ rad. Figure 9 shows the roll angle response versus time. It can be seen that the model is close to the experimental data during the initial phase of the response with a similar rise time. The first peak value is smaller, but the next two peak values are close. The period of oscillation is also accurate. The final part of the response including the equilibrium point is accurate, although the damping is too small at the end of the response. This deviation in damping in the final part of the response was also observed in the identification section. Overall, the agreement is relatively close and comparable to the agreement for the data set used for identification of the parameters (see Fig. 6). The main aspect of deviation appears to be with the damping being somewhat too small in the final phase of the response. This does not appear to result in large deviations in the roll angle, however, as it occurs at the end of the response where the amplitude of oscillation is relatively small. In future work, this aspect of the approach is one possible area for improvement. Figure 10 shows the time history of the left and right vortex breakdown locations. It can be seen that the vortex breakdown locations take place symmetrically to the midchord of the wing when the delta wing reaches its equilibrium point. The equilibrium point will thus be close to zero. It can be seen that the vortex breakdown locations from the simulation are relatively close to the experimental values, especially during the initial phase. The rise time, peak values, and period of oscillation are also similar. The final part of the response is close, including the equilibrium values.

The data set for IC 4 had initial conditions of $\phi(t) = -0.69$ rad for all $t \leq 0$ with an equilibrium point of $\phi_e = -0.36$ rad. Figure 11 shows the roll angle response versus time. It is apparent that the overall simulation response is similar to the experimental data. There is some deviation in the initial response, including a higher initial peak value, but the peak time and initial period of oscillation are similar. The final part of the response has some small deviations as a result of the period of oscillation being somewhat too small in the final part of the response. However, the equilibrium value is very

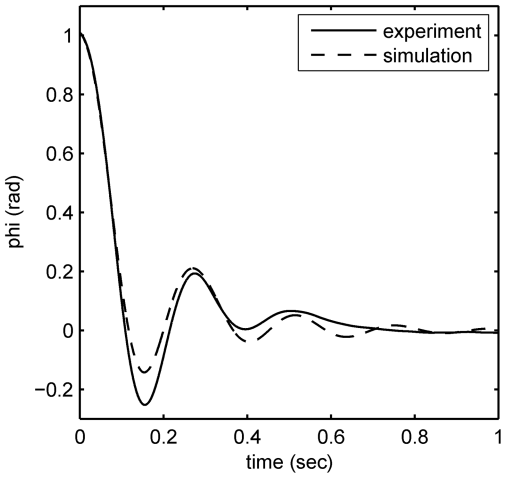

Fig. 9 Roll angle vs time (IC 3).

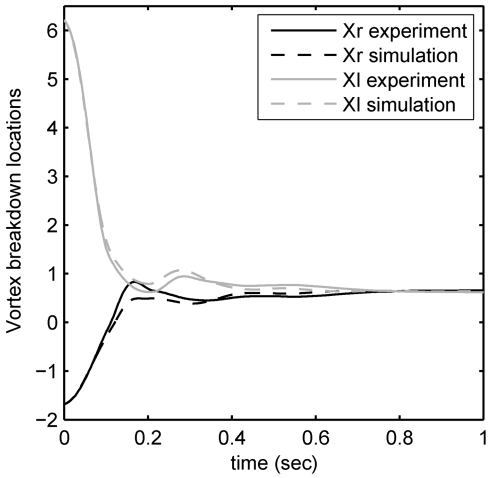

Fig. 10 Left and right vortex breakdown locations (IC 3).

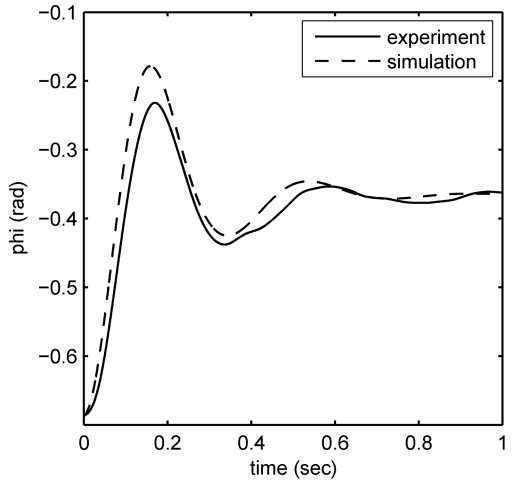

Fig. 11 Roll angle vs time (IC 4).

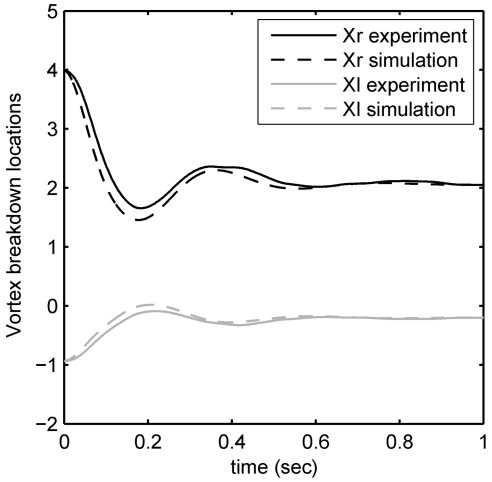

Fig. 12 Left and right vortex breakdown locations (IC 4).

close. The damping for the initial and final parts of the response were also similar to the experimental data. The agreement for this data set is relatively close and comparable to the agreement for the data set used for identification of the parameters (see Fig. 8). Figure 12 shows the time history of the left and right vortex breakdown locations. The right vortex breakdown location takes place far beyond the trailing edge of the wing when the equilibrium point is reached. It can be seen that the vortex breakdown locations of the simulation are similar to the experimental values. The initial peak values are slightly larger, but the period of oscillation is similar and the final phase of the response is close, including the equilibrium values.

It is apparent from the results presented in this section that the experimental data validate the proposed delta wing model for data sets that were not used in the identification process. The proposed model captures the main dynamic behavior of the system including peak times, periods of oscillation, and the respective equilibrium points. It should also be noted that the proposed model was validated for the case where no input is applied to the system. In future work, as more experimental data becomes available, the proposed model will be experimentally validated for conditions with control inputs applied to the system.

VII. Conclusions

In this paper, a new state-space model for vortex-coupled delta wing aircraft systems is developed, based on a modified nonlinear indicial response method combined with an internal state-space representation. Least-squares identification of the proposed model was performed for various initial conditions. Three different methods were tested for the approximation of the rolling moment coefficient: linear, fifth-order polynomial, and static approximation. It was found that the fifth-order polynomial method provided close agreement to experimental data for a number of different initial conditions. This experimentally validated state-space model represents a significant step toward a control-oriented model for vortex-coupled delta wing systems. The experimental data currently available provided validation of the proposed model for the case with no input applied to the system. In future work, the proposed model will be experimentally validated for conditions with control inputs applied to the system.

Acknowledgments

This work was supported in part by the Natural Sciences and Engineering Research Council of Canada and Defence Research and Development Canada under the project entitled Supersonic Missile Flight Control by Manipulation of the Flow Structure Using Micro-Actuated Surfaces. The authors would also like to thank X. Z. Huang of National Research Council Canada for providing experimental data and helpful scientific advice.

References

[1] Lee, G. B., Shih, C., Tai, Y. C., Tsao, T., Liu, C., Huang, A., and Ho, C. M., "Robust Vortex Control of a Delta Wing by Distributed Microelectromechanical-Systems Actuators," *Journal of Aircraft*, Vol. 37, No. 4, July–Aug. 2000, pp. 697–705. doi:10.2514/2.2655

[2] Huang, P. H., Folk, C., Silva, C., Christensen, B., Chen, Y. F., Lee, G. B., Chen, Minjdar, Newbern, S., Jiang, F., Grosjean, C., Ho, C. M., and Tai, Y. C., "Applications of MEMS Devices to Delta Wing Aircraft: From Concept Development to Transonic Flight Test," AIAA Paper No. 2001-0124, Jan. 2001.

[3] Folk, C., and Ho, C. M., "Micro-Actuators for Control of Delta Wing with Sharp Leading Edge," AIAA Paper No. 2001-0121, Jan. 2001.

[4] Huang, X. Z., Sun, Y. Z., and Hanff, E. S., "Circulation Criterion to Predict Leading Edge Vortex Breakdown Over Delta Wings," AIAA Paper 1997-2265, 1997.

[5] Huang, X. Z., and Hanff, E. S., "Prediction of Normal Force on a Delta Wing Rolling at High Incidence," AIAA Paper 93-3686, Aug. 1993.

[6] Chaderjian, N. M., and Schiff, B., "Numerical Simulation of Forced and Free-to-Roll Delta Wing Motions," *Journal of Aircraft*, Vol. 33, No. 1, 1996, pp. 93–99. doi:10.2514/3.46908

[7] Juang, J. N., Kholodar, D., and Dowell, E. H., "System Identification of a Vortex Lattice Aerodynamic Model," NASA TM-2001-211229, Oct. 2001.

[8] Greenwell, D. I., "Simple Engineering Model for Delta-Wing Vortex Breakdown," *Journal of Aircraft*, Vol. 40, No. 2, 2003, pp. 402–405. doi:10.2514/2.3110

[9] Tobak, M., Chapman, G. T., and Schiff, L. B., "Mathematical Modeling of the Aerodynamic Characteristics in Flight Dynamics," NASA TM-85880, 1984.

[10] Huang, X. Z., Lou, H. Y., and Hanff, E. S., "Non-Linear Indicial Response and Internal State-Space Representation for Free-to-Roll Trajectory Prediction of a 65° Delta Wing at High Incidence," AIAA Paper 2002-4713, 2002.

[11] Huang, X. Z., "Non-Linear Indicial Response/Internal State-Space Representation and Its Applications on Delta Wing Aerodynamics," *21st Applied Aerodynamics Conference*, AIAA Paper 2003-3944, June 2003.

[12] Greenwell, D., "A Review of Unsteady Aerodynamic Modelling for Flight Dynamics of Manoeuvrable Aircraft," *AIAA Atmospheric Flight Mechanics Conference and Exhibit*, AIAA Paper 2004-5276, Aug. 2004.

[13] Reisenthel, P. H., and Bettencourt, M. T., "Extraction of nonlinear indicial and critical state responses from experimental data," *37th Aerospace Sciences Meeting and Exhibit*, AIAA Paper 1999-764, Jan. 1999.

[14] Reisenthel, P. H., "Development of a Nonlinear Indicial Model for Maneuvering Fighter Aircraft," AIAA Paper 96-0896, 1996.

[15] Reisenthel, P. H., "Application of Nonlinear Indicial Modeling to the Prediction of a Dynamically Stalling Wing," AIAA Paper 96-2493, 1996.

[16] Reisenthel, P. H., "Development of a Nonlinear Indicial Model Using Response Functions Generated by a Neural Network," AIAA Paper 97-0337, 1997.

[17] Reisenthel, P. H., and Bettencourt, M. T., "A Nonlinear Indicial Prediction Tool for Unsteady Aerodynamic Modeling," AIAA Paper 98-4350, 1998.

[18] Reisenthel, P. H., Xie, W., Gursul, I., and Bettencourt, M. T., "An Analysis of Fin Motion Induced Vortex Breakdown," AIAA Paper 99-0136, 1999.

[19] Reisenthel, P. H., and Bettencourt, M. T., "Data-Based Aerodynamic Modeling Using Nonlinear Indicial Theory," AIAA Paper 99-0763, 1999.

[20] Reisenthel, P. H., and Bettencourt, M. T., "Extraction of Nonlinear Indicial and Critical State Response from Experimental Data," AIAA Paper 99-0764, 1999.

[21] Pamadi, B. N., Murphy, P. C., Klein, V., and Brandon, J. M., "Prediction of Unsteady Aerodynamic Coefficients at High Angles of Attack," AIAA Paper 2001-4077, Aug. 2001.

[22] Reisenthel, P. H., "Prediction of Unsteady Aerodynamic Forces via Nonlinear Kernel Identification," *CEAS/AIAA/ICASE/NASA Langley International Forum on Aeroelasticity and Structural Dynamics*, Nelson Engineering & Research Paper 379June 1999.

[23] Klein, V., and Noderer, K. D., "Modeling of Aircraft Unsteady Aerodynamic Characteristics, Part 1: Postulated Models," NASA TM 109120, May 1994.

[24] Goman, M., and Khrabrov, A., "State-Space Representation of Aerodynamic Characteristics at High Angles of Attack," *Journal of Aircraft*, Vol. 31, No. 5, Sept.–Oct. 1994, pp. 1109–1115. doi:10.2514/3.46618

[25] Smith, T. A., and Hakanson, J. W., Nair, S. S., Yurkovich, R. N., "State-Space Model Generation for Flexible Aircraft," *Journal of Aircraft*, Vol. 41, No. 6, Nov.–Dec. 2004, pp. 1473–1481. doi:10.2514/1.14433

[26] Murphy, P. C., and Klein, V., "Estimation of Aircraft Unsteady Aerodynamic Parameters from Dynamic Wind Tunnel Testing," AIAA Paper 2001-4016, 2001.

[27] Tobak, M., and Schiff, L. B., "Aerodynamic Mathematical Modeling: Basic Concepts," NASA Center for AeroSpace Information (CASI), Hanover, MD, 1981, AGARD Dynamic Stability Parameters, p. 31, Document ID 19810022564.

[28] Schiff, L. B., Tobak, M., and Malcolm, G. N., "Mathematical Modeling of the Aerodynamics of High-Angle-of-Attack Maneuvers," *Atmospheric Flight Mechanics Conference*, AIAA Paper 80-1583, Aug. 1980.

[29] Jenkins, J. E., Myatt, J. H., and Hanff, E. S., "Body-Axis Rolling Motion Critical States of a 65 Degree Delta Wing," *Journal of Aircraft*, Vol. 33, No. 2, March–April 1996, pp. 268–278. doi:10.2514/3.46933

[30] Grismer, D. S., and Jenkins, J. E., "Critical States Transients for a Rolling 65 Degree Delta Wing," *Journal of Aircraft*, Vol. 34, No. 3, May–June 1997, pp. 380–386. doi:10.2514/2.2180

[31] Allwine, D. A., Strahler, J. A., Lawrence, D. A., Jenkins, J. E., and Myatt, J. H., "Nonlinear Modeling of Unsteady Aerodynamics at High Angle of attack," *AIAA Atmospheric Flight Mechanics Conference and Exhibit*, AIAA Paper 2004-5275, Aug. 2004.

[32] Huang, X. Z., Lou, H. Y., and Hanff, E. S., "Non-Linear Indicial Response and Internal State-Space Representation for Free-to-Roll Trajectory Prediction of a 65° Delta Wing at High Incidence," AIAA Paper 2002-4713, 2002.

[33] Richard, J. P., "Time-Delay Systems: An Overview of Some Recent Advances and Open Problems," *Automatica*, Vol. 39, No. 10, 2003, pp. 1667–1694. doi:10.1016/S0005-1098(03)00167-5

[34] Ericsson, L. E., "Flow Physics of Critical States for Rolling Delta Wings," *Journal of Aircraft*, Vol. 32, No. 3, May–June 1995, pp. 603–610. doi:10.2514/3.46762

[35] Ericsson, L. E., "Difficulties in Predicting Vortex Breakdown Effects on a Rolling Delta Wing," *Journal of Aircraft*, Vol. 33, No. 3, May–June 1996, pp. 477–484. doi:10.2514/3.46969

[36] Ericsson, L. E., and Hanff, E. S., "Further Analysis of High-Rate Rolling Experiments of a 65-Deg Delta Wing," *Journal of Aircraft*, Vol. 31, No. 6, Nov.–Dec. 1994, pp. 1350–1357. doi:10.2514/3.46658

[37] Greenwell, D. I., and Wood, N. J., "Static Roll Moment Characteristics of Asymmetric Tangential Leading Edge Blowing on a Delta Wing at High Angles of Attack," AIAA Paper 93-0052, Jan. 1993.

[38] Greenwell, D. I., and Wood, N. J., "Roll Moment Characteristics of Asymmetric Tangential Leading Edge Blowing on a Delta Wing," *Journal of Aircraft*, Vol. 31, No. 1, Jan.–Feb. 1994, pp. 161–168. doi:10.2514/3.46469

[39] Myatt, J. H., and Arena, A. S., "A Theoretical/Empirical Model for Rolling Delta Wings with Vortex Breakdown," AIAA Paper 98-2527, 1998.

[40] Ericsson, L. E., and Beyers, M. E., "Aspects of Ground Facility Interference on Leading-Edge Vortex Breakdown," *Journal of Aircraft*, Vol. 38, No. 2, 2001, pp. 310–314. doi:10.2514/2.2763

[41] Ericsson, L. E., "Difficulties in Predicting Vortex Breakdown Effect on a Rolling Delta Wing," *Journal of Aircraft*, Vol. 33, No. 3, May–June 1996, pp. 477–484. doi:10.2514/3.46969

[42] Menke, M., Yang, H., Gursul, I., "Experiments on the Unsteady Nature of Vortex Breakdown over Delta Wings," *Experiments in Fluids*, Vol. 27, No. 3, 1999, pp. 262–272. doi:10.1007/s003480050351

[43] Ericsson, L. E., "Effect of Fuselage Geometry on Delta-Wing Vortex Breakdown," *Journal of Aircraft*, Vol. 35, No. 6, Nov.–Dec. 1998, pp. 898–904. doi:10.2514/2.2410

[44] Reisenthel, P. H., and Bettencourt, M. T., "Data-Based Aerodynamic Modeling Using Nonlinear Indicial Theory," *37th Aerospace Sciences Meeting and Exhibit*, AIAA 1999-763, Jan. 1999.

[45] Reisenthel, P. H., Bettencourt, M. T., Myatt, J. H., and Grismer, D. S., "A Nonlinear Indicial Prediction Tool for Unsteady Aerodynamic Modeling," *AIAA Atmospheric Flight Mechanics Conference and Exhibit*, AIAA Paper 1998-4350, Aug. 1998.

[46] Eykhoff, P., *System Identification, Parameter and State Estimation*, Wiley, New York, 1974.

[47] Haykin, S., *Neural Networks a Comprehensive Foundation*, Second Ed., Prentice–Hall, Upper Saddle River, NJ, 1999, pp. 256–317.

[48] Sanner, R. M., and Slotine, J. J. E., "Gaussian Networks for Direct Adaptive Control," *IEEE Transactions on Neural Networks*, Vol. 3, No. 6, Nov. 1992, pp. 837–863. doi:10.1109/72.165588

[49] Huang, X. Z., "Experimental Investigation of Leading Edge Vortex Control via Microactuators," *Missile Flight Control Using Micro-Actuated Flow Effectors Meeting*, Defense Research and Development Canada, TN 2004-066, May 2004.